CHAPTER III
NUMERICAL CALCULATION

3.1 Mathematical Approach

In this section, the theoretical calculation procedures as well as the mathematics behind the calculation are discussed. The mathematical model for the calculation was based on the AFM images of the LAQD system and on the results obtained from the PL measurements. It was observed that the quantum dots aligned in the $[1\bar{1}0]$ direction and that the size in the [001] direction (the growth direction) of each QD was 4 nm and the sizes in the [110] and $[1\bar{1}0]$ directions were both about 40 nm to 60 nm for aligned quantum dots, and about 20 nm for binary quantum dots. Generally, strong PL signal comes from the recombination between electrons and holes in the ground state, thus the main focus of the calculation was on the ground-state eigen-energy levels.

3.2 Mathematical Model

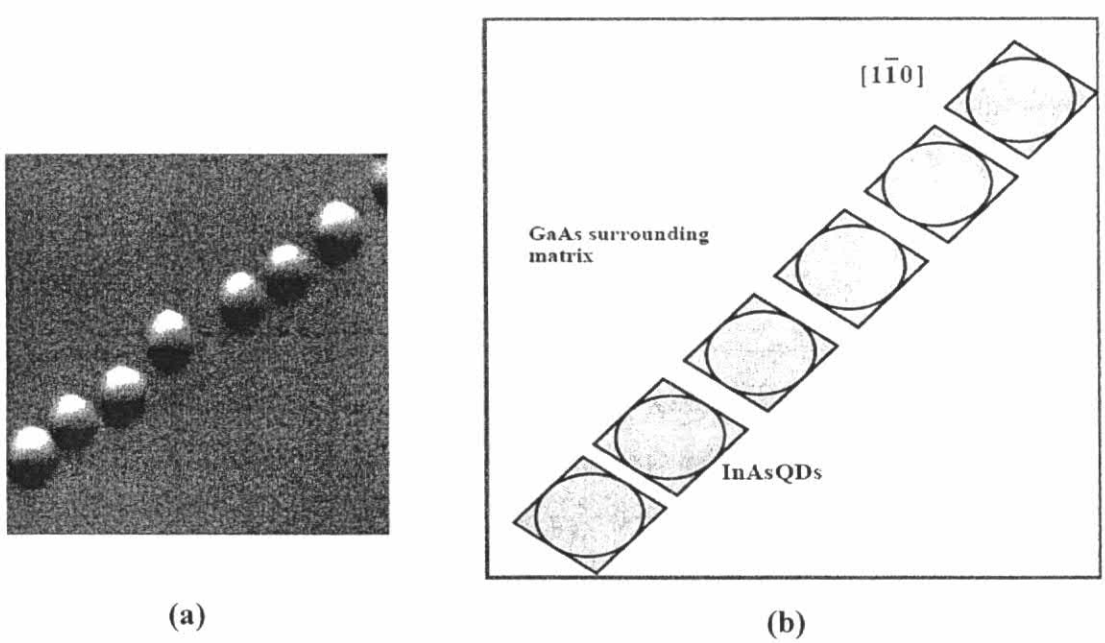

Figure 3.1 (a) An AFM image of InAs/GaAs linearly aligned quantum dots, and (b) the corresponding schematic diagram.

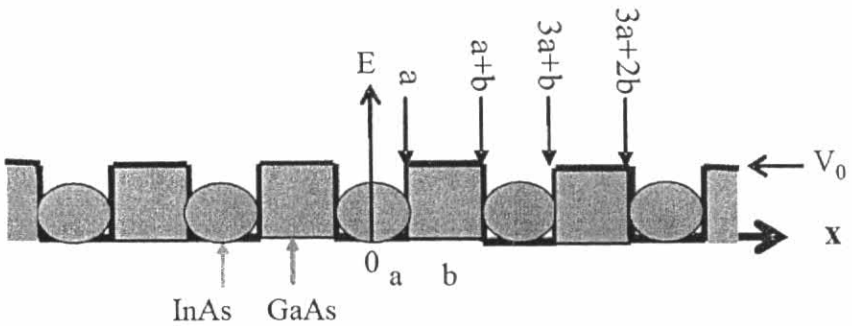

Figure 3.2 Schematic diagram of the model for linearly aligned quantum dots.

According to the AFM image, the top view of the QDs has a circular shape. The InAs QDs were embedded in the GaAs surrounding matrix (i.e., GaAs capping layer and substrate). In the calculation it was assumed for simplicity that all the QDs had the same size with the same spacing between them, so that the quantum-mechanical model of the LAQD system is similar to that of the periodic multiple quantum wells, as shown in Fig. 3.2, in which the quantum well regions correspond to the InAs quantum dots and the potential barriers correspond to the GaAs capping-layer material.

3.3 Theory

Since the quantum dots aligned along a straight line and the PL from them showed a certain degree of linear polarization, the relevant Schrödinger equation is one-dimensional, with three describing parameters, namely, the well width of size $2a$, the barrier width b, and the barrier height V_0. In as much as the PL is due mainly to the recombination of carriers in the ground state, the calculation was focused on the ground-state eigen-energies (E_0) only. The eigen-energy and the eigen-function (wavefunction) of a single carrier in semiconductor linearly aligned quantum dots can be calculated from the time-independent Schrödinger equation:

$$H\psi(x) = [-\frac{\hbar^2}{2m^*}\frac{\partial^2}{\partial x^2} + V(x)]\psi(x) = E\psi(x) \qquad (3.1)$$

In the above Eq. (3.1), m^* is the effective mass of the electron and $\hbar$ is the Planck's constant. $V(x)$ is the difference between the bandgap energy of InAs quantum

dots and the GaAs surrounding matrix, which are 1.12 eV and 1.43 eV (at room temperature), respectively. That is,

$$V(x) = \begin{cases} 0 & \begin{cases} x \in QDs \\ x \notin QDs \end{cases} \\ V_0 \end{cases}$$

$\psi(x)$ is the wavefunction that satisfies the appropriate boundary conditions. E is the eigen-energy of the system. Since recombination occurs for the carriers in the *bound states*, only the case for which $E < V_0$ was considered.

3.4 Numerical Method

The Schrödinger equation was solved using the finite difference method (FDM) written in the Matlab® programming language. The FDM was implemented using uniform grids for the one- and two-dimensional Schrödinger equations in rectangular coordinates.

3.4.1 One-Dimensional Schrödinger Equation

To solve the Eq. 3.1 numerically by using FDM, the wavefunction must be discretized first [50]. The wavefunction and the potential were discretized into many small grid points such that the x coordinates becomes $x_i = ih_0$, where the index $i = 0, 1, 3$ 4, , N (arbitrary integer), and h_0 is the separation between the adjacent grid points. This is illustrated in Fig. 3.3.

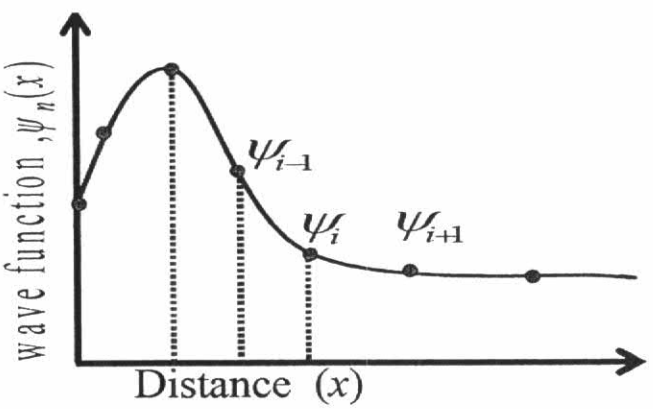

Figure 3.3 Three-point finite-difference approximation used to discretize the wavefunction and the potential energy.

By using a three-point finite-difference approximation, the second derivative of the discretized wavefunction became

$$\frac{d^2}{dx^2}\psi(x_i)=\frac{\psi(x_{i+1})-2\psi(x_i)+\psi(x_{i-1})}{h_0^2} \tag{3.2}$$

After substituting Eq. 3.2 into 3.1, the following matrix equation was obtained:

$$H\psi(x)=[-u_i\psi(x_{i+1})+d_i\psi(x_i)-u_i\psi(x_{i-1})]=E\psi(x_i) \tag{3.3}$$

In Eq. 3.3, the Hamiltonian is a symmetric tri-diagonal matrix. The diagonal matrix elements are

$$d_i=\frac{\hbar^2}{mh_0^2}+V(i) \tag{3.4}$$

and the adjacent off-diagonal matrix elements are

$$d_i=\frac{\hbar^2}{2mh_0^2} \tag{3.5}$$

Changing Eq. 3.3 into a matrix form yields the following equation

$$(H-EI)\psi=\begin{bmatrix} (d_1-E) & -u_2 & . & . & . & . & & \\ -u_2 & (d_2-E) & -u_3 & . & & & & \\ . & -u_3 & (d_3-E) & -u_4 & . & & & \\ . & . & -u_4 & (d_4-E) & . & . & & \\ . & . & & & . & . & & \\ . & . & & & . & . & . & \\ . & & & & . & . & & \\ & & & & & -u_{N-1} & (d_1-E) & \end{bmatrix}\begin{bmatrix} \psi_1 \\ \psi_2 \\ \psi_3 \\ \psi_4 \\ \\ \\ \\ \psi_{N-1} \end{bmatrix}=0 \tag{3.6}$$

where H is the Hamiltonian matrix and I is the identity matrix. By using Matlab® programming language the eigen-energies and eigen-functions of the one-dimensional quantum well problem were obtained.

For the present purpose, the semiconductor heterostructure model was used, and so the different effective masses were taken into account. Ben-Daniel and Duke's effective mass Hamiltonian was used in the Schrödinger equation:

$$H = -\frac{\hbar^2}{2}\frac{\partial}{\partial x}\left(\frac{1}{m^*(x)}\frac{\partial}{\partial x}\right) + V(x) \tag{3.7}$$

Discretization of the Schrödinger equation using Ben-Daniel and Duke's effective Hamiltonian [51-53] gives

$$\frac{-\hbar^2}{x^2}\left(\frac{\psi_{j+1}}{m^*_{i+1}+m^*_i} - \frac{\psi_j}{m^*_{i+1}+m^*_i} - \frac{\psi_j}{m^*_{i-1}+m^*_i} + \frac{\psi_{j-1}}{m^*_{i-1}+m^*_i}\right) + V_j\psi_i = E\psi_i \tag{3.8}$$

Eq. (3.8) can be constructed in a matrix form similar to the previous equation.

3.4.2 Two-Dimensional Rectangular Dots

For the two-dimensional case, the Hamiltonian of the Schrödinger equation has two variables.

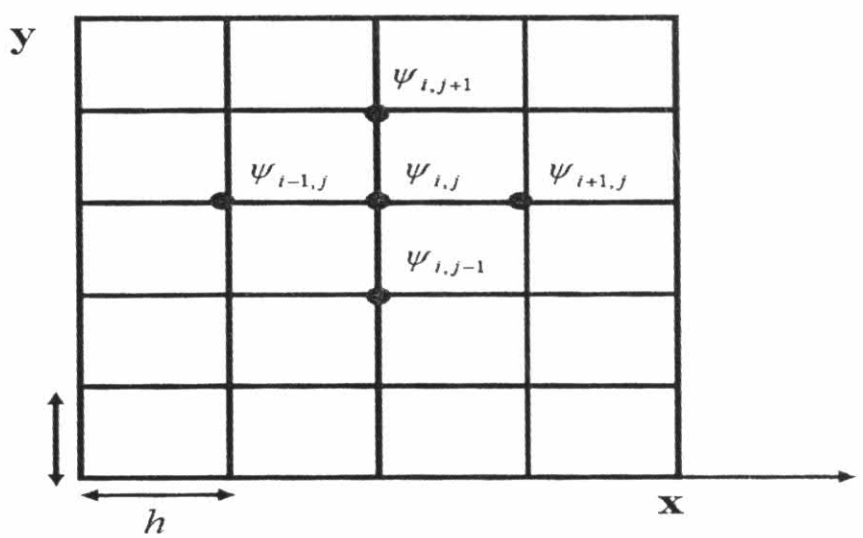

Figure 3.4 The discretized mesh points for the two-dimensional Schrödinger equation.

The two-dimensional Schrödinger equation was changed into the two-dimensional finite-difference form:

$$-\frac{\hbar^2}{2m^* h_0^2}\left[\{\psi_{i-1,j}-2\psi_{i,j}+\psi_{i+1,j}\}-2\psi_{i,j}+\{\psi_{i,j-1}-2\psi_{i,j}+\psi_{i,j+1}\}\right]+V_{ij}\psi_{i,j}=E\psi_{i,j} \tag{3.9}$$

Using different effective masses in the above equation leads to:

$$\frac{-\hbar^2}{h_0^2}\left(\frac{\psi_{i,j-1}}{m^*_{i,j-1}+m^*_{i,j}}+\frac{\psi_{i,j+1}}{m^*_{i,j+1}+m^*_{i,j}}+\frac{\psi_{i-1,j}}{m^*_{i-1,j}+m^*_{i,j}}+\frac{\psi_{i+1,j}}{m^*_{i+1,j}+m^*_{i,j}}-\right.$$
$$\left.\frac{\psi_{ij}}{m^*_{i,j+1}+m^*_{i,j}}-\frac{\psi_{ij}}{m^*_{i+1,j}+m^*_{i,j}}-\frac{\psi_{ij}}{m^*_{i-1,j}+m^*_{i,j}}-\frac{\psi_{ij}}{m^*_{i,j+1}+m^*_{i,j}}\right)+V_j\psi_i=E\psi_{ij} \tag{3.10}$$

The above differential equation can be changed into the following matrix form:

$$\begin{bmatrix}
(d_{11}-E) & -u & & u & & & & & \\
-u & (d_{12}-E) & -u & & u & & & & \\
 & -u & (d_{13}-E) & & & u & & & \\
u & & & (d_{21}-E) & -u & & u & & \\
 & u & & -u & (d_{22}-E) & -u & & u & \\
 & & u & & -u & (d_{23}-E) & -u & & u \\
 & & & u & & -u & (d_{31}-E) & & \\
 & & & & u & & & (d_{32}-E) & -u \\
 & & & & & u & & -u & (d_{33}-E)
\end{bmatrix}\begin{bmatrix}\psi_{11}\\ \psi_{21}\\ \psi_{31}\\ \psi_{12}\\ \psi_{22}\\ \psi_{32}\\ \psi_{13}\\ \psi_{23}\\ \psi_{33}\end{bmatrix}=0 \tag{3.11}$$

Checking the Numerical Method

To check the accuracy of the numerical method thus developed, an analytical method was used for comparison. For simplicity, the binary QD system was considered. The wavefunctions and the derivative of the wavefunctions of the QDs were continuous at the boundaries. After manipulating the Hamiltonian equation, a transcendental equation was obtained. By using the graphical method or an aide by the computer program, the eigen-energies and eigen-functions of the system can be

obtained. By comparing these results with the numerical data, the accuracy of the numerical method could be then adjusted.

Table 3.1: Comparison between the analytical and the numerical methods.

Eigen-energy level	Analytical method	FDM 200 node points/nm	FDM 100 node points/nm	FDM 50 node points/nm
E_1	1.13573399	1.135722787087	1.135689165755	1.135554701534
E_2	1.159285852	1.159274775287	1.159241544238	1.159108640738
E_3	3.970491881	3.970465351407	3.970384186515	3.970059481673
E_4	4.203528034	4.203498010204	4.203398998420	4.203002901767

The results above are the four lowest eigen-energies of a bi-QD system with the well width 2 nm, the barrier width 2 nm, and the barrier high 5 eV. A 4000 × 4000 matrix was the largest matrix used in the calculations. From the above table, it can be clearly seen that the higher number of node points, the better the accuracy is.

3.5 Results and Discussion

3.5.1 Energy-Splitting Behavior

A computer program was written in Matlab® to numerically solve the equation that was written by Finite-Difference Method (FDM) with appropriate boundary conditions. Fig. 3.5 (a), (b) and (c) show the ground-state energy E_0 as a function of the barrier width b, for fixed values of the well width $2a$ = 20 nm and the barrier height V_0 = 0.31 eV, corresponding to the chain of four, five, and six quantum dots, respectively. As shown in Fig. 3.5, for fixed values of the well width and barrier height, the ground-state energy levels begin to split when the potential wells are close enough to each other so that coupling between them manifests, and the energy levels become degenerate when the wells are far enough from each other so that the coupled dots become similar to the single, individual dots. Note that in any case the splitting is maximum when the barrier width is zero (no barrier), in other words, all the quantum wells coalesce and become a single longer potential well having an integral

size of $n(2a)$, where n is the number of the constitutive wells. When this happens the top-most and the bottom-most of the splitting energy levels are identical to the first excited-state and ground-state energy levels of a single, isolated potential well of size $n(2a)$, respectively. Higher energy levels obtained from these calculations also show a similar trend.

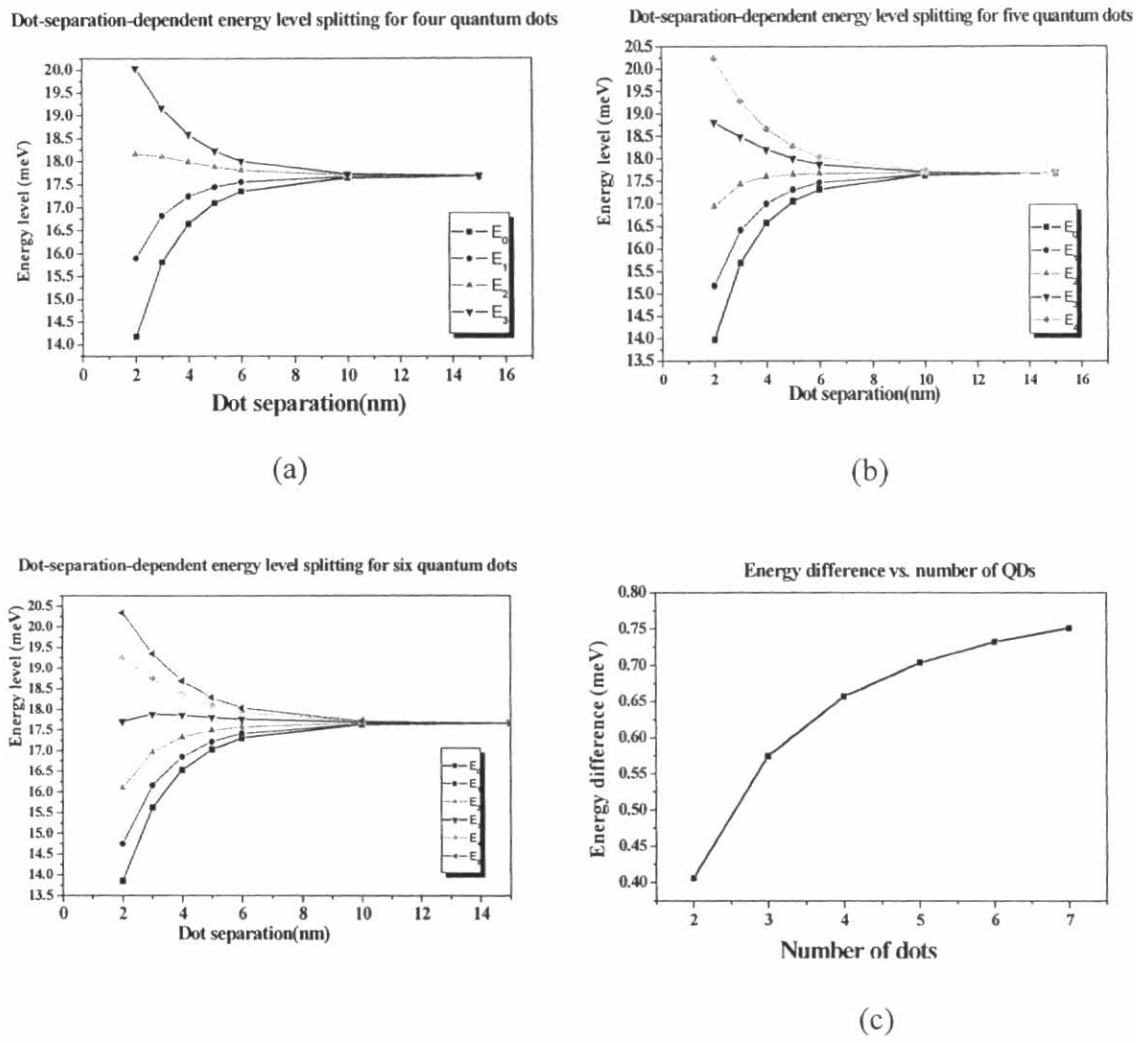

Figure 3.5 Dot-separation-dependent energy splitting behavior for (a) four, (b) five, and (c) six QDs; and (d) difference in energy of the top-most and the bottom-most ground-state levels versus the number of QDs.

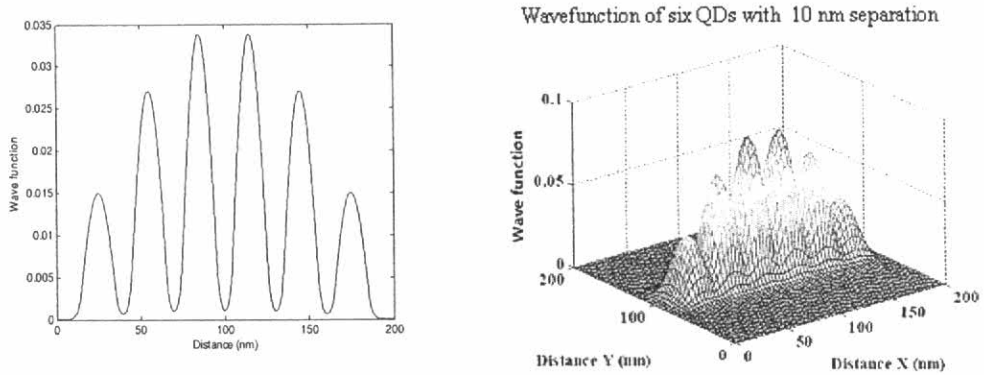

(a)

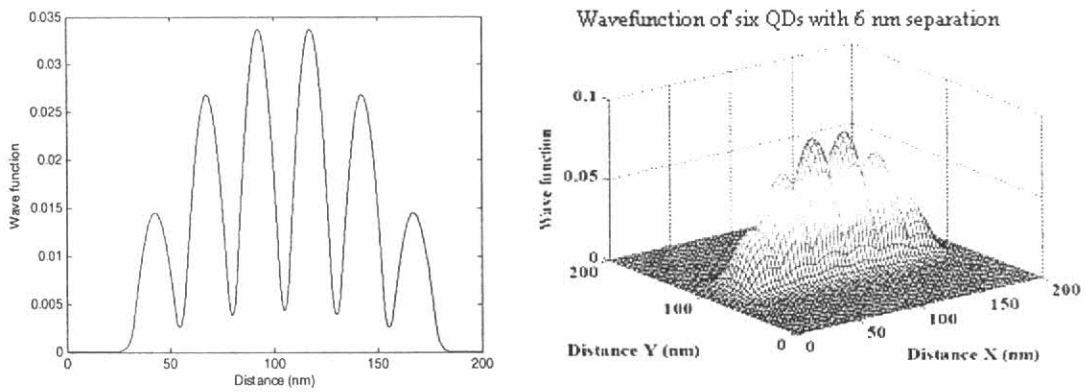

(b)

Figure 3.6 One-dimensional (left) and two-dimensional (right) coupling behavior of six coupled QDs with dot separation (a) 10 nm, and (b) 6 nm.

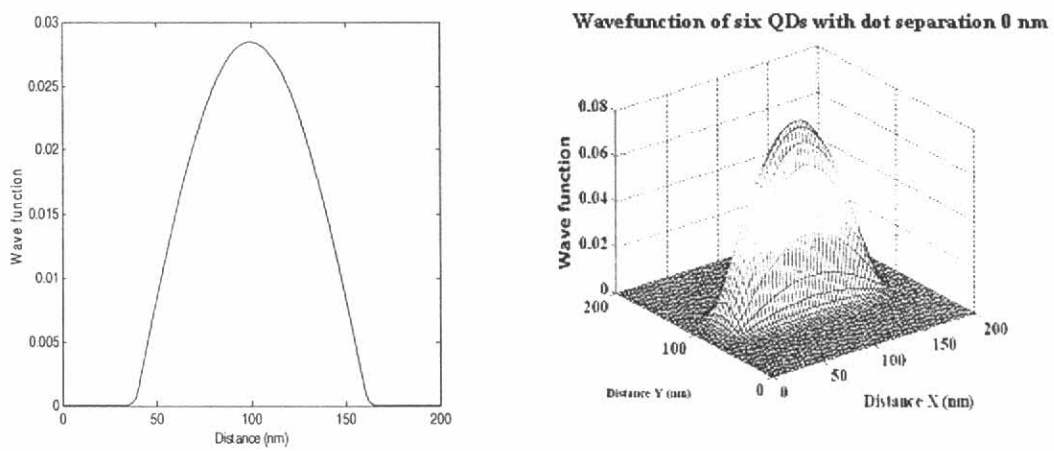

Figure 3.7 The maximum coupling caused by coalescence of six coupled QDs.

The coupling behavior of QDs can be clearly seen from the shape of the wavefunctions in the one-dimensional as well as in the two-dimensional case, as shown in Figs. 3.6 and 3.7. For the case of six square-shaped coupled quantum dots whose side is $2a$ = 20 nm, when the dot separation is 10 nm, coupling between the dots may be already seen, as in the Fig. 3.6 (a). When the dot separation becomes smaller, e.g., 6 nm, coupling between the dots becomes more pronounced, as in Fig. 3.6 (b). Coupling is maximum when the dots completely fuse together (zero separation), as shown in Fig. 3.7, and in this case the QD system looks like a quantum wire.

According to the calculations and the results obtained above, the coupling and energy splitting behaviors depend on separation between quantum dots. Controlling the energy splitting of the system is interesting for the polarization property. Polarization characteristic is to some extent related to the energy splitting and coupling among aligned quantum dots.

3.5.2 Effect of Coupling on the Linear Optical Polarization Property

The energy splitting of any coupled QD system is significant in the direction of the dot alignment. As the number of dots increases, the amount of energy splitting also increases. In two dimensions, if the quantum dots align, say, in the x direction, then the splitting of energy levels is significant in the x direction, there is virtually not much energy splitting in the y direction. Significant energy splitting in the x direction implies dominant linear polarization in the x direction. For a two-dimensional system, the optical intensity due to carrier transitions within the system may be found from the expression:

$$I_{if}^{(\theta)} \propto \int \psi_i(x,y) r_\theta \psi_f(x,y) dxdy \tag{3.12}$$

where r stands for the coordinate of the optical transition, θ stands for either the x or the y direction of polarization of light, ψ_i is the ground-state electron wavefunction, and ψ_f is the ground-state hole wavefunction. If QDs align in the x direction, the major contribution to the optical transition is the x component of the wavefunctions. By using the above equation, the degree of optical polarization anisotropy, or in short the "polarization degree" (PD) for two-dimensional systems may be determined as

$$PD = \left| \frac{I^x - I^y}{I^x + I^y} \right| \tag{3.13}$$

where I^x and I^y are the emission optical intensity in x and y direction, respectively.

3.5.2.1 Single Quantum Dots

First, single quantum dots of an isotropic shape (12 nm×12 nm) as well as elongated quantum dots whose size in the y direction was fixed to 12 nm and that in the x direction varied from 12 nm to 108 nm were investigated. The ground-state wavefunctions of the electron and the hole were calculated by solving Schrödinger equation using the finite-difference method, in which a uniform mesh was used in the x and y directions and 2 nm was equivalent to 1 mesh. The largest matrix size for this two-dimensional calculation was 3600 × 3600. The calculated electron wavefunction for isotropic quantum dots and elongated quantum dots are as shown in Fig. 3.8 and 3.9 respectively. Here, x and y directions correspond to the $[1\bar{1}0]$ and [110] directions, respectively.

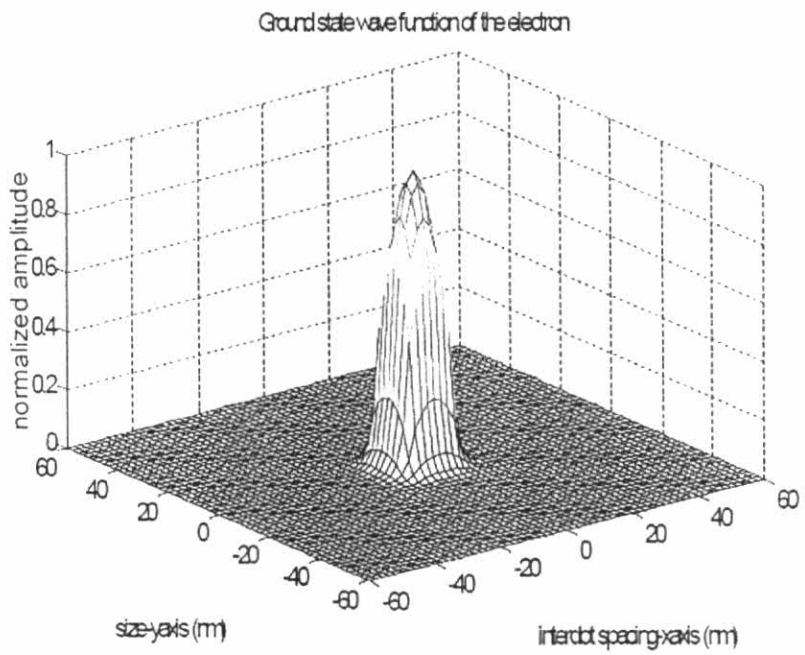

Figure 3.8 The ground-state electron wavefunction of an isotropic single quantum dot whose size is 12 nm × 12 nm.

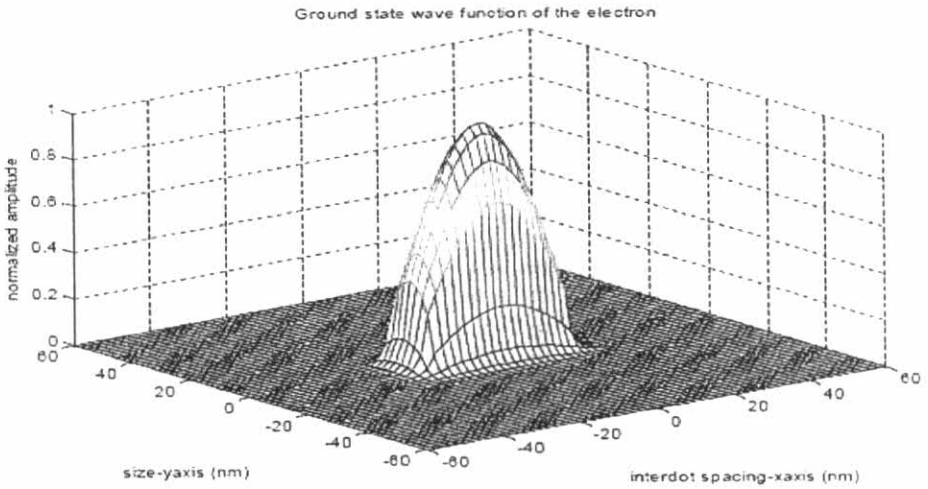

Figure 3.9 The ground-state electron wavefunction of an elongated QD (the size in the x direction was elongated to 36 nm while that in the y direction was maintained at 12 nm).

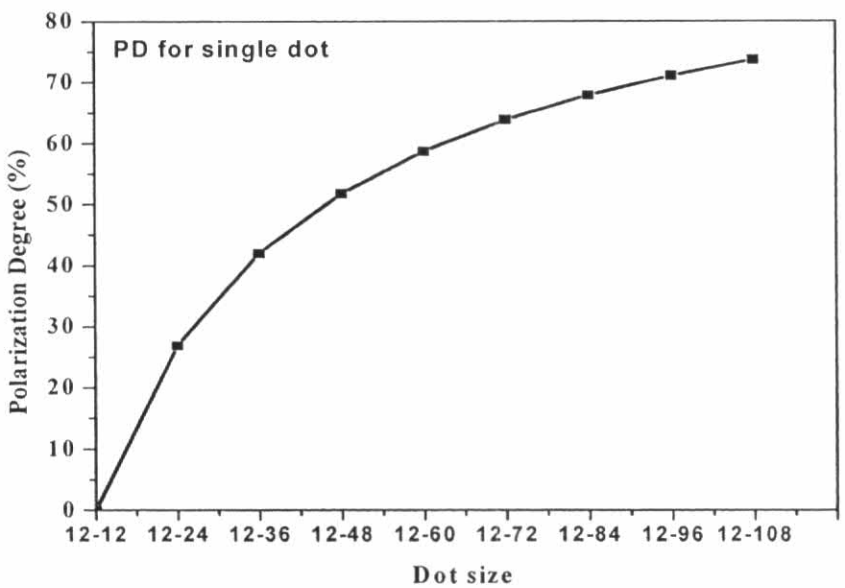

Figure 3.10 The polarization degree for a single QD whose size in the x direction was elongated from 12 nm to108 nm while that in the y direction was maintained at 12 nm.

Table 3.2: The polarization degree vs. dot aspect ratio of single QDs.

Dot aspect ratio (nm-nm)	**Polarization degree (%)**
12-12	0
12-24	24.88
12-36	41.92
12-48	51.97
12-60	58.92
12-72	64.14
12-84	67.61
12-96	71.85
12-108	73.96

The above calculation results (Table 3.2) show that when the size of the quantum dot is isotropic, that is, the size in the x and y directions are the same, then the transition probability in the x and the y directions are the same. For this case, the degree of polarization is zero. When the size of the quantum dot is elongated in the x direction, the transition in the x and the y directions are not the same. Elongated quantum dots thus show a certain degree of linear polarization (PD $\neq$ 0). When the dot size is elongated more and more in a certain direction, the PD increases.

3.5.2.2 Binary Quantum Dots

The wavefunctions in Figs. 3.12 and 3.13 are the calculation results which show the ground-state electron wavefunction of binary quantum dots which are aligned in the x direction, that is, the $[1\,\bar{1}0]$ direction. There was some barrier thickness between the two quantum dots and this thickness needed to be taken into account in the calculation. The spatial separation of the barrier strongly affects the "overlap integral" Γ, which measures the amount of overlapping between electron and hole wavefunctions and is defined as

$$\Gamma = \frac{\int_{-\frac{a}{2}}^{\frac{a}{2}} \int_{-\frac{d}{2}}^{\frac{d}{2}} \psi_e(x,y) \cdot \psi_h(x,y) dxdy}{\int_{-\frac{a}{2}}^{\frac{a}{2}} \int_{-\frac{d}{2}}^{\frac{d}{2}} dxdy} \tag{3.14}$$

where ψ_e is the ground-state wavefunction of the electron and ψ_h is the ground-state wavefunction of the hole. By integrating the dot product between the electron and the hole wavefunctions over all space, the overlap integral for the electron and hole wavefunctions was obtained. Here, d and a are the spatial separation and the size of the QDs, respectively. The schematic diagram for the above equation is depicted in Fig. 3.11.

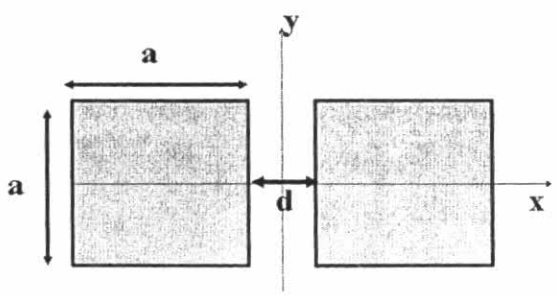

Figure 3.11 Schematic diagram of binary quantum dots, each of size **a**×**a** nm^2 and interdot spacing **d** nm.

Finally, the polarization degree for the bi-QDs may be calculated by

$$PD = \Gamma \times \left| \left(\frac{I^x - I^y}{I^x + I^y} \right) \right| \tag{3.16}$$

Eq. 3.16 was modified from Eq. 3.13 only by the multiplicative factor Γ, which needs to be taken into account for any coupled-QD systems. The degree of linear polarization (PD) of the binary quantum dots was calculated by using this last formula. Next, the number of quantum dots was increased in the *x* direction, while for the *y* direction only one dot was maintained. The thickness of the barrier between the two quantum dots in the *x* direction plays important role to determine the polarization degree of binary quantum dots. When the thickness of the barrier is smallest, the highest PD is obtained. The polarization degree tends to increase when the spatial separation between the two quantum dots decreases (see Table 3.3 and 3.14).

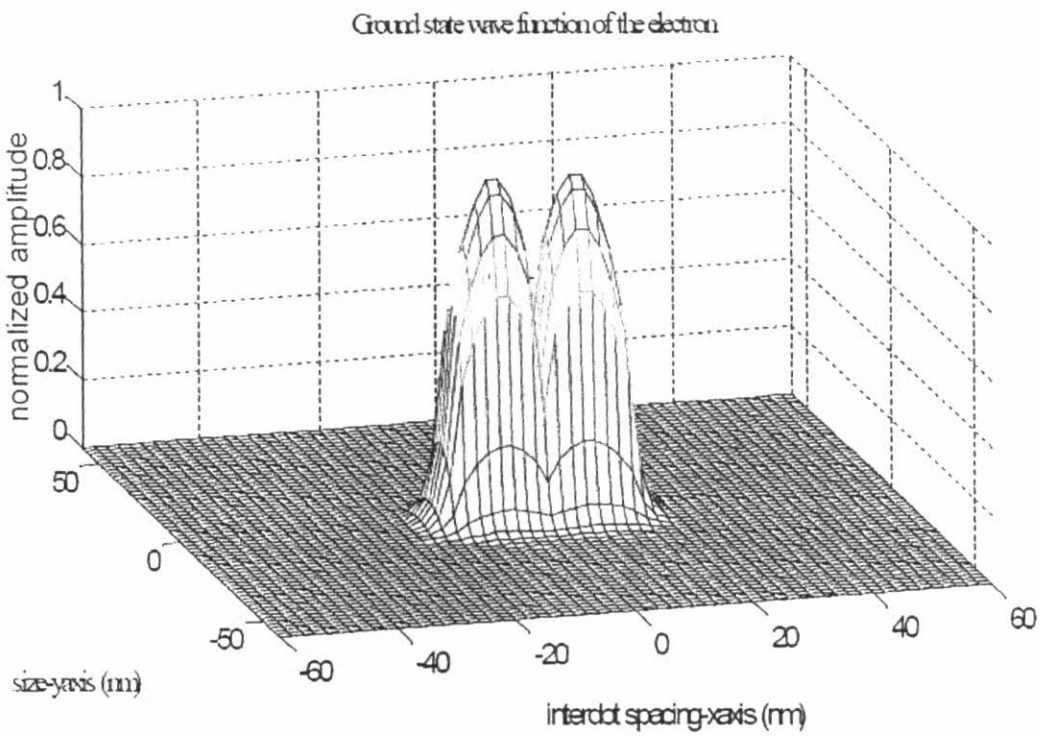

Figure 3.12 The ground-state electron wavefunction of binary quantum dots, each of size 12 nm × 12 nm with an interdot spacing of 2 nm.

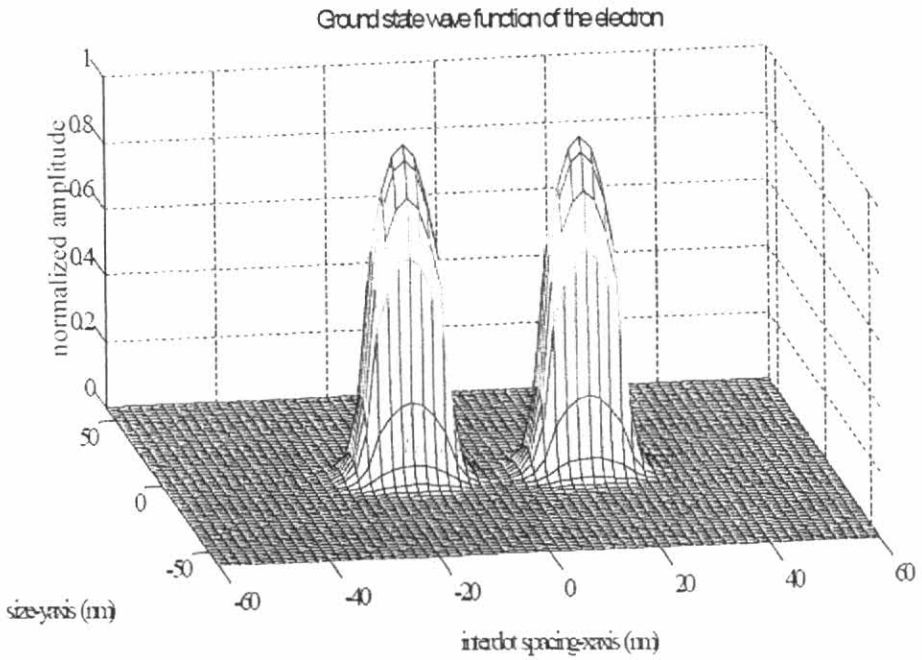

Figure 3.13 The ground-state electron wavefunction of binary quantum dots, each of size 12 nm × 12 nm with an interdot spacing of 12 nm.

Table 3.3: The polarization degree of binary quantum dots with various interdot spacings. The middle number refers to the interdot spacing that is, the barrier width between the dots.

Dot structure (nm-nm-nm)	**Polarization degree (%)**
12-0-12	26.88
12-2-12	13.44
12-6-12	6.12
12-10-12	4.40
12-14-12	3.51
12-18-12	2.95
12-22-12	2.55

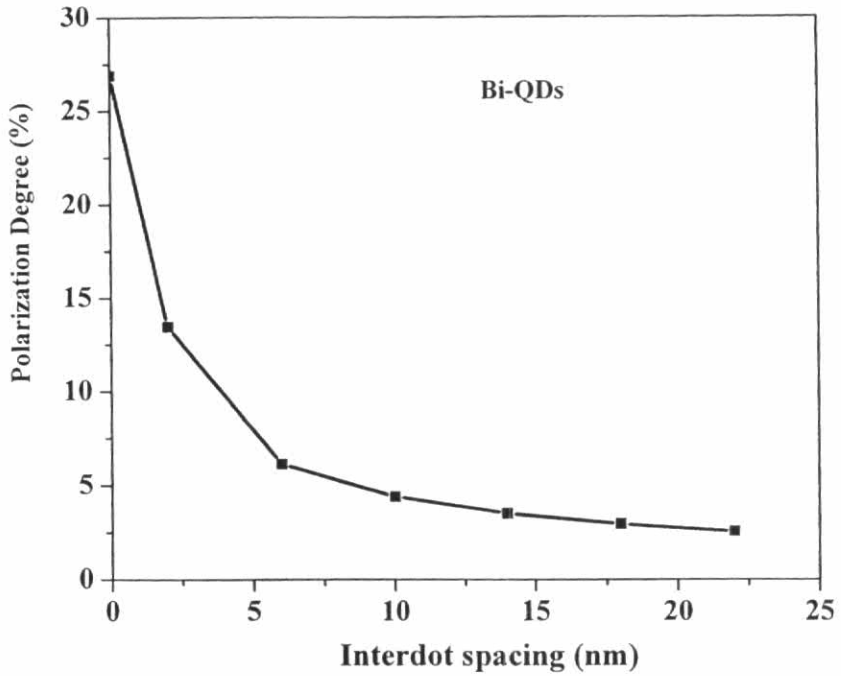

Figure 3.14 The polarization degree of binary quantum dots vs. their interdot spacing (the dot size was fixed at 12 nm × 12 nm and the interdot spacing was varied from 0 nm to 22 nm).

Table 3.4: The polarization degree of binary quantum dots with various dot sizes. The dot size was varied from 8 nm to 44 nm while the interdot spacing was fixed at 2 nm.

Dot size (nm-nm)	Polarization degree (%)
8-8	20.41
12-12	13.44
16-16	9.52
20-20	7.11
24-24	5.22
28-28	4.41
32-32	3.61
36-36	3.02
40-40	2.54
44-44	2.18

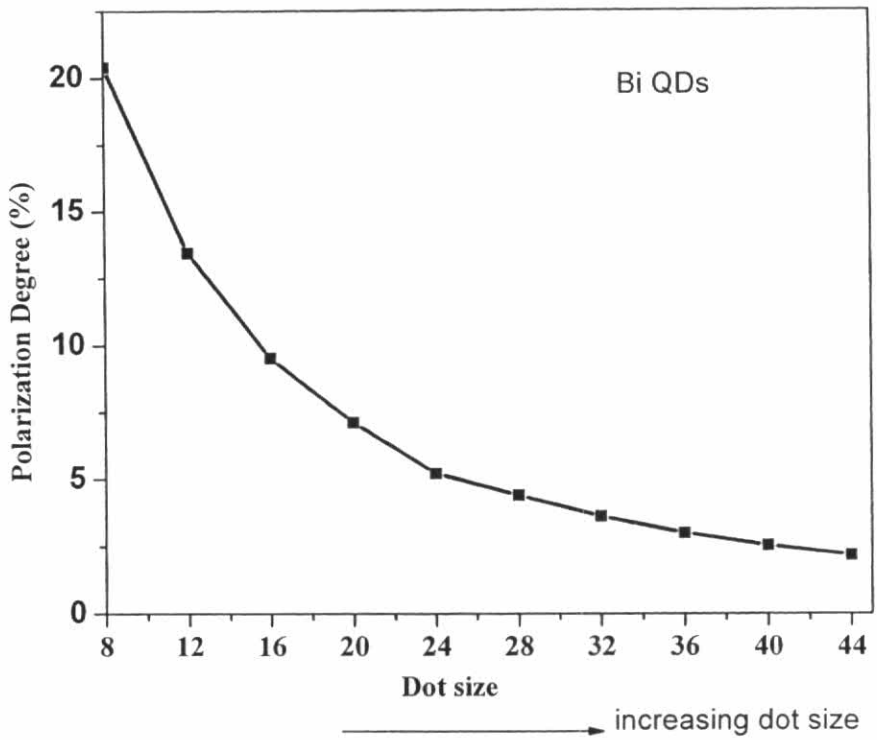

Figure 3.15 The polarization degree of binary quantum dots with various dot sizes. The dot size was varied from 8 nm to 44 nm while interdot spacing was fixed at 2 nm.

3.5.2.3 Increase of Polarization Degree with Number of QDs

Next, the number of the quantum dots aligned in the *x* direction was varied from two to seven quantum dots. In other words, the number of quantum dots was increased in the *x* direction and for the *y* direction the only one quantum dot was maintained. In this case, the thickness of the barrier, or the spacing, between aligned quantum dots was maintained at 2 nm. The degree of linear polarization of multiple aligned quantum dots was still calculated by using Eq. (3.16). It was found that when the number of quantum dots increased, the degree of polarization also increased, as shown in Table 3.5 and Fig. 3.16.

Table 3.5: The polarization degree vs. the number of QDs aligned in the *x* direction. The dot size was maintained at 12 nm × 12 nm (isotropic shape) and the interdot spacing between adjacent QDs was fixed at 2 nm. The number of dots increased in the *x* direction.

Number of dots	Polarization degree (%)
1	0.00
2	13.44
3	22.20
4	26.12
5	28.20
6	29.44
7	30.87

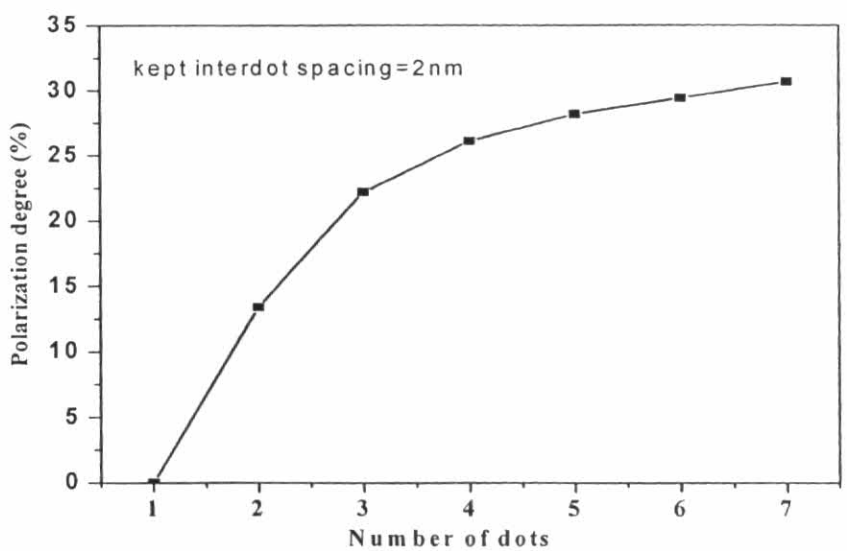

Figure 3.16 The polarization degree vs. the number of QDs aligned in the *x* direction. The dot size was maintained at 12 nm × 12 nm (isotropic shape) and the interdot spacing between adjacent QDs was fixed at 2 nm. The number of dots increased in the *x* direction.

3.6 Conclusion

The degree of linear polarization (PD) of the PL spectrum emitted from QD system was theoretically calculated by using the Schrödinger equation implemented using the finite-difference method (FDM). The degree of polarization is zero when the single dot has an isotropic shape. A certain degree of polarization is obtained when the dot is elongated in one direction. For binary quantum dots and linearly aligned quantum dots, the polarization degree strongly depends on spatial separation between adjacent dots. When the interdot spacing is smallest, the highest degree of polarization is obtained. The size of the individual quantum dots in the coupled system also affects the degree of polarization. See Table 3.5 and Fig. 3.15. Smaller quantum dots show a larger degree of coupling, and hence a larger degree of polarization. For larger isotropic quantum dots, the wave function is confined in the dot region and so the amount of wave function overlapping is small. In conclusion, to get a larger degree of linear polarization from the aligned quantum dots, a smaller dot size, and a very close spacing between adjacent dots, and a long dot alignment are preferred.